

An Interpretable Latent Denoising Diffusion Probabilistic Model for Fault Diagnosis Under Limited Data

Tian Zhang, Jing Lin, *Senior Member, IEEE*, Jinyang Jiao, *Member, IEEE*, Han Zhang, and Hao Li

***Abstract*—Despite the remarkable success of end-to-end intelligent diagnosis methods, the shortage of available training data remains one of the most challenging issues in real industrial scenarios. In light of this, a wide variety of deep generative models are developed for data volume expansion. Notably, the denoising diffusion probabilistic model (DDPM) has recently shown impressive sample quality and diversity in various tasks. However, DDPM typically operates in the original pixel space, resulting in an expensive computational cost and restricting its applicability in industrial applications. In tackling the above issues, we develop an interpretable vector quantization-guided latent denoising diffusion probability model (IVQ-LDM) in this work. In IVQ-LDM, the vector quantized-variational autoencoder is introduced to compress the data to a lower dimensional space, where the kernels with physical meaning are then designed in the first layer to enhance the density of latent information and improve model interpretability. After that, a conditional DDPM is built in this latent space to learn the low-dimensional representation for data augmentation. Compared with existing methods, the IVQ-LDM achieves enhancements in sample quality, computational efficiency, and interpretability. Extensive experiments on three mechanical systems corroborate the effectiveness and superiority of the proposed method.**

***Index Terms*—Denoising diffusion probabilistic model, intelligent fault diagnosis, interpretability, limited data, variational autoencoder (VAE).**

I. Introduction

WITH the flourishing development of industrial information technology and artificial intelligence, deep learning has created new opportunities for condition monitoring of industrial equipment. Given the inevitable faults of machines, implementing effective health management strategies is essential for extending the equipment service life while safeguarding both economic benefits and personal security [1], [2]. Following this trend, various remarkable achievements have been provided in deep learning-based machine fault diagnosis [3], [4], [5].

Although tremendous progress, the data-hungry nature of deep neural networks restricts their further development to some extent. In many studies, sufficient training data is necessary for establishing accurate intelligent diagnosis models [6], [7]. Nevertheless, collecting ample high-quality fault data in real-case scenarios is impractical for the following reasons. 1) Machines will be shut down immediately for maintenance once a sudden failure occurs. 2) Manually labeling large amounts of data incurs expensive costs in terms of time and human labor [8]. These factors undoubtedly pose a severe challenge to researching high-precision and well-generalized models.

In response to the aforementioned issues, data generation techniques provide a direct and effective way to enlarge the original dataset. At present, variational autoencoder (VAE) and generative adversarial networks (GAN) are commonly used generative model frameworks. Nonetheless, the effectiveness of VAE is restricted by the Gaussian prior assumptions in generating authentic samples [9]. In contrast, the excellent portability and data generation quality of GAN make it a popular solution for the data scarcity dilemma, with various variants continually emerging [10], [11]. For example, Liu et al. [12] solved the data scarcity problem by incorporating the self-attention mechanism into the GAN. Shao et al. [13] established a dual-attention GAN and leveraged the infrared thermal images for bearing fault diagnosis with small data. Zhang et al. [14] presented a multimodule GAN improved by an adaptive decoupling strategy to address the lack of monitoring data. Despite the marvelous success in intelligent fault diagnosis, GAN-based data generation strategies are often considered challenging to train and susceptible to mode collapse due to their adversarial mechanism [15].

Given the limitations of the above existing generative models, we introduce a novel concept for fault data generation, i.e., the denoising diffusion probabilistic model (DDPM). This model exhibits extraordinary performance and training stability in many computer vision tasks [16], [17]. Specifically, DDPM is a parameterized Markov process trained using variational inference to produce samples matching the original data. Noise is

Manuscript received 7 October 2023; accepted 26 March 2024. Date of publication 10 May 2024; date of current version 5 August 2024. This work was supported in part by the National Natural Science Foundation of China under Grant 52205080 and Grant 52235002, and in part by the Science and Technology on Reliability and Environmental Engineering Laboratory Foundation under Grant 6142004210501. Paper no. TII-23-3879. *(Corresponding author: Jinyang Jiao.)*

Tian Zhang, Jing Lin, Jinyang Jiao, and Hao Li are with the School of Reliability and Systems Engineering, Beihang University, Beijing 100191, China (e-mail: tian@buaa.edu.cn; linjing@buaa.edu.cn; jiaojinyang@buaa.edu.cn; buaalihao@buaa.edu.cn).

Han Zhang is with the Institute of Mechanics and Acoustics, National Institute of Metrology, Beijing 100029, China (e-mail: zhh@nim.ac.cn).

Color versions of one or more figures in this article are available at https://doi.org/10.1109/TII.2024.3393002.

Digital Object Identifier 10.1109/TII.2024.3393002

the transfer medium of this chain, which is viewed as a learnable variable that is iteratively diffused and denoised until it is completely removed to recover the original input. However, since the DDPM primarily operates in the pixel space, optimizing powerful DDPM requires expensive computational resources [18]. To reduce the computational overhead of DDPM while ensuring its performance, we leverage the dimensionality compression property of convolutional autoencoders and introduce a vector quantization (VQ) mechanism to enhance the performance of autoencoders [19]. We present a vector quantization-based latent diffusion model (VQ-LDM) for fault data generation. The diffusion process is applied to low-dimensional data in the latent discrete space of the vector quantized-variational autoencoder (VQ-VAE).

Another limitation of deep generative models for fault diagnosis is the lack of interpretability, which does not offer insight into how and what knowledge the neural network has learned. In this case, the network may consume some resources to extract unknown or even meaningless information, compromising its credibility and effectiveness. Recently, the interpretable convolution kernels ensemble strategy has been explored and demonstrated its effectiveness in various tasks. Ravanelli et al. [20] achieved efficacy in speech recognition tasks through an interpretable convolution kernels ensemble. Zhang et al. [21] efficiently extract fault-related information from lamb waves by establishing interpretable kernels with toneburst signal form. Inspired by this, we introduce this idea into the VQ-LDM by designing interpretable convolution kernels embedded with fault impact form, thereby enhancing the density of fault-related information in the latent space.

By consolidating the VQ-based latent denoising diffusion probabilistic model and interpretable convolution kernels, we propose a novel interpretable vector quantization-guided latent denoising diffusion probabilistic model (IVQ-LDM) for machinery fault diagnosis under limited data. As far as we know, our work is the first attempt to introduce the diffusion generation concept in the fault diagnosis community. The major contributions of this work are as follows.

1) We present a novel framework, i.e., IVQ-LDM, for data generation in machinery fault diagnosis under limited data, which could perceptually learn the latent distribution of the fault data.
2) Our IVQ-LDM introduces the dimensionality compression strategy, which improves computational efficiency while ensuring the data generation quality.
3) We introduce the interpretable concept into the generative model and leverage it to improve the density of fault-related information in the latent space, thereby enhancing the quality of generated data and model interpretability.
4) Comprehensive experiments and comparative studies are conducted on three mechanical systems to validate the superiority of the proposed IVQ-LDM.

The rest of this article is organized as follows. Section II introduces the theoretical basis of the DDPM and VQ-VAE. Section III details the proposed IVQ-LDM. Next, Section IV reports the experimental and analytical results. Finally, Section V concludes this article.

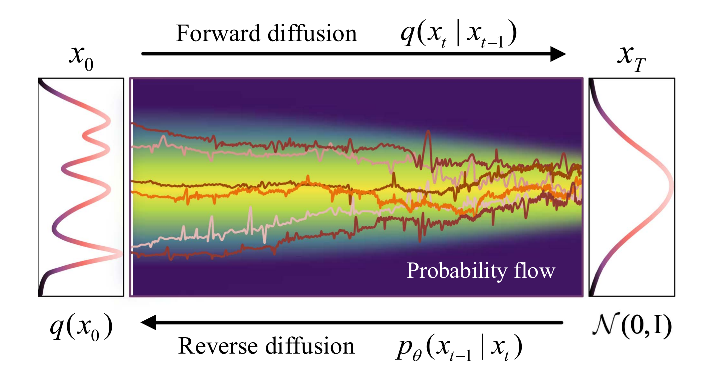


Fig. 1. Learning process of the denoising diffusion probabilistic model.

II. Theoretical Basis

A. Denoising Diffusion Probability Model

DDPM [16] consists of two parameterized Markov chains and utilizes variational inference to generate samples matching the original data distribution after finite iteration times. The diagram of the learning process of DDPM is shown in Fig. 1. The forward diffusion chain disturbs the data by adding Gaussian noise through a predesigned schedule until the distribution converges to a given standard Gaussian prior. The reverse diffusion chain learns to gradually recover the undisturbed data structure starting from the given prior. This is a process of learning how to generate data by continually destroying and rebuilding it. Formally, given a training sample $x_0 \sim q(x_0)$, we define the forward Markovian diffusion process q which produces the noised versions $x_1, x_2, \ldots, x_T$ by adding Gaussian noise at step t according to a variance schedule $\beta_1, \beta_2 \ldots, \beta_T$ as follows:

$$q(x_1, x_2, \ldots, x_T|x_0) = \prod_{t=1}^{T} q(x_t|x_{t-1}) \quad (1)$$

$$q(x_t|x_{t-1}) = \mathcal{N}\left(x_t; \sqrt{1-\beta_t}x_{t-1}, \beta_t \mathrm{I}\right), \beta_t \in (0,1) \quad (2)$$

where $q(x_t)$ represents the data distribution at the diffusion step t in the forward diffusion process; I is the identity matrix having the same dimensions as the input data x_0; $\mathcal{N}(x; \mu, \sigma)$ denotes the Gaussian distribution of the mean μ and variance σ that produces x. The noising process referred to (1) allows us to directly sample the diffused data x_t at an arbitrary step t of the forward process.

With the notation $\alpha_t = 1 - \beta_t$and $\bar{\alpha}_t = \Pi_{s=1}^{t} \alpha_s$, we have

$$\begin{aligned} q(x_t|x_0) &= \int q(x_{1:t}|x_0) dx_{1:(t-1)} \\ &= \mathcal{N}(x_t; \sqrt{\bar{\alpha}_t}x_0, (1-\bar{\alpha}_t)\mathrm{I}) \end{aligned} \quad (3)$$

so that we can express any intermediate step x_t with a linear combination of x_0 and a noise variable ε

$$x_t = \sqrt{\bar{\alpha}_t}x_0 + \sqrt{1-\bar{\alpha}_t}\varepsilon, \ \varepsilon \sim \mathcal{N}(0, \mathrm{I}). \quad (4)$$

When $\bar{\alpha}_T$ sufficiently close to 0, $q(x_T|x_0)$ will converge to a Gaussian prior distribution, i.e., $p(x_T) \approx \mathcal{N}(x_T; 0, \mathrm{I})$. The joint distribution $p_\theta(x_{0:T})$ is called the reverse Markovian diffusion

process starting from $p(x_T)$. We can thus parameterize this process as follows:

$$p_\theta(x_{0:T}) = p(x_T) \prod_{t=1}^{T} p_\theta(x_{t-1}|x_t) \tag{5}$$

$$p_\theta(x_{t-1}|x_t) = \mathcal{N}(x_{t-1}; \mu_\theta(x_t, t), \Sigma_\theta(x_t, t)) \tag{6}$$

where $p_\theta(x_t)$ represents the probability distribution of variables x_t in the reverse process; $\mu_\theta(x_t, t)$ denotes the learnable mean functions of reversed diffusion process at step t; $\Sigma_\theta(x_t, t)$ is the learnable variance at reversed step t; θ is the parameter that is learned to fit the data distribution $q(x_0)$ by optimizing the variational lower bound on negative log-likelihood

$$\begin{aligned}
&\max_\theta \mathbb{E}_{q(x_0)} [\log p_\theta(x_0)] \\
&\leq \max_\theta \mathbb{E}_{q(x_0,\ldots,x_T)} [\log p_\theta(x_{0:T}) - \log q(x_{1:T}|x_0)] && (7)\\
&= \max_\theta \mathbb{E}_{q(x_0,\ldots,x_T)} \left[-\log p(x_T) - \sum_{t\geq 1} \log \frac{p_\theta(x_{t-1}|x_t)}{q(x_t|x_{t-1})} \right] && (8)
\end{aligned}$$

where $\mathbb{E}$ represents the expected value. As for $p_\theta(x_{t-1}|x_t)$, if the variance $\Sigma_\theta(x_t, t)$ is fixed to constant values $\sigma_t^2 = \beta_t$, the objective referred to (8) can be simplified to

$$\mathcal{L}(\varepsilon_\theta) = \sum_{t=1}^{T} \mathbb{E}_{x_0,\varepsilon,t} \left[||\varepsilon_t - \varepsilon_\theta(x_t, t)||_2^2 \right] \tag{9}$$

where ε_θ is a trainable neural network, and $\varepsilon_\theta(x_t, t)$ is a network predicting the noise ε that can generate x_t. Then, the mean of noise $\mu_\theta(x_t, t)$ in the reverse process can be expressed as

$$\mu_\theta(x_t, t) = \frac{1}{\sqrt{\alpha_t}} \left(x_t - \frac{\beta_t}{\sqrt{1 - \bar{\alpha}_t}} \varepsilon_\theta(x_t, t) \right). \tag{10}$$

Eventually, in the inference stage, we can sample and generate data starting from the normal variables step by step, as follows:

$$x_{t-1} = \frac{1}{\sqrt{\alpha_t}} \left(x_t - \frac{\beta_t}{\sqrt{1 - \bar{\alpha}_t}} \varepsilon_\theta(x_t, t) \right) + \sigma_t z, \ \ z \sim \mathcal{N}(0, \mathrm{I}). \tag{11}$$

B. Vector Quantized-Variational Autoencoder

Due to the expensive computational cost of the original DDPM, we opt to leverage the dimensionality compression strategy of the autoencoder. Compared with traditional autoencoders that rely on continuous latent variables, VQ-VAE utilizes discrete latent representations, which have been demonstrated to be more effective in many generation tasks [19]. In addition, it gets rid of the usual posterior collapse issue in VAE. Formally, the model comprises an encoder E, a decoder D and a codebook $B = \{e_k\}_{k=1}^{K} \in \mathbb{R}^{K\times d}$ containing a certain number of latent embedding vectors. Given an input sample $x \in \mathbb{R}^{W\times 1}$, we obtain the continuous latent variable z_e with the encoder $z_e = E(x)$, which is subsequently quantized to z_q based on its distance to the embedding vectors B

$$z_q = e_k \in \mathbb{R}^{w\times d}, k = \arg\min_j ||z_e - e_j||_2^2 \tag{12}$$

where z_q stands for the final coding vectors; w denotes the length of each latent vector; d represents the depth of each embedding in the codebook. Then, the reconstructed data can be obtained by feeding the vectors into the decoder. Particularly, the VQ process is nondifferentiable, the gradient reconstruction technology using straight-through operation is employed to backpropagate the gradient. At last, the regularized commitment loss is applied to keep the training stable, which encourages the output of the encoder close to the selected codebook vectors. The VQ-VAE can be trained end-to-end via the following objective:

$$\begin{aligned}
\mathcal{L}_{VQ} = &\ \|x - D(z_q)\|_2^2 + \|\mathrm{sg}\,[E(x)] - z_q\|_2^2 \\
&+ \zeta \, \|sg\,[z_q] - E(x)\|_2^2
\end{aligned} \tag{13}$$

where $\mathrm{sg}[\cdot]$ represents the stop-gradient operation; ζ is the trade-off hyperparameter.

III. Proposed Method

In this section, we first state the concerned issue. Then, the proposed IVQ-LDM with dimensionality compression strategy and interpretable kernel ensemble is presented and introduced in detail. The framework of IVQ-LDM is depicted in Fig. 2.

A. VQ-LDM With Dimensionality Compression

Due to the expensive computation cost of vanilla DDPM, the dimensionality compression strategy based on VQ-VAE is introduced in this work. The latent representation z_e of the original signals can be obtained through encoder $E$from the pretrained VQ-VAE. Then, the VQ regularization is applied for fine-tuning the latent feature to obtain the z_q referred to (12).

With the above processes, we can now efficiently access to a low-dimensional latent representation space, where more abstracted detail information with a higher density of key features can be acquired. The DDPM is subsequently employed for learning the representation of the latent feature distribution. According to the forward Markovian process of DDPM, the latent feature is diffused to $z_{q,t}$ through the randomly selected diffusion step $t \in [1, 2, \ldots, T]$ and predefined variance schedule β. In the reverse denoising learning stage, a denoising U-net with parameter θ is applied to learn the noise level from the diffusion step $t-1$ to t by the objective function referred to (9).

In addition, the controllable generation for a single generative model is of great practical benefit in fault diagnosis. The DDPM is capable of modeling the conditional distribution of the form $p_\theta(z_{q,t-1}|z_{q,t}, y)$ with the labels y. In this work, the conditional input is acted on the upsampling stage of the denoising U-net. Finally, the training objective for VQ-LDM can be expressed by

$$\begin{aligned}
&\mathcal{L}_{\mathrm{VQ-LDM}} \\
&\quad = \mathbb{E}_{z_{q,0},\varepsilon,t} \left[\left\| \varepsilon_t - \varepsilon_\theta \left(\sqrt{\bar{\alpha}_t} z_{q,0} + \sqrt{1 - \bar{\alpha}_t} \varepsilon, t, y \right) \right\|_2^2 \right].
\end{aligned} \tag{14}$$

At last, the recovered latent representations can be obtained step by step from random variables referred to (11), and subsequently fed into the VQ-VAE decoder to generate new data.

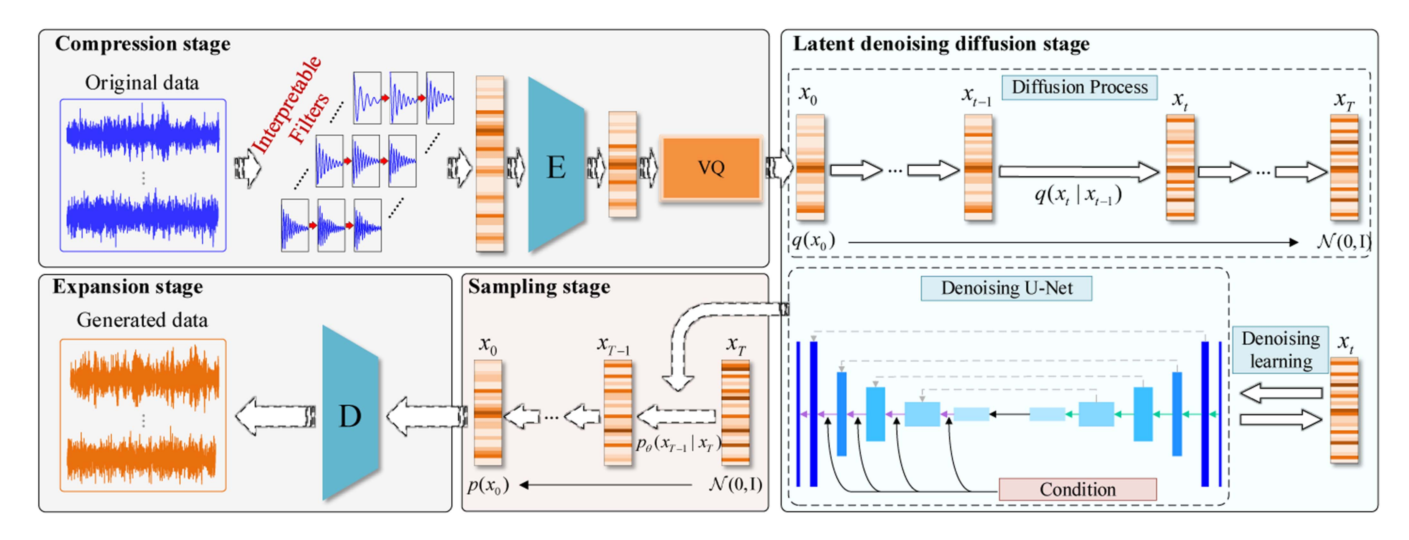


Fig. 2. Main learning framework of IVQ-LDM. E and D is the encoder and decoder of the VQ-VAE respectively. The hollow arrows indicate the feature flow.

B. Perceptual Compression With Interpretable Kernel

Limited by the black-box nature of the deep learning models, the generative models usually treat all input features equally, which makes it difficult to effectively extract the key information. More importantly, we introduce the diffusion generation strategy into the hidden layers, which may compromise the performance of DDPM if the effective information density is low. This will result in more resources being exhausted for learning random and irrelevant information, and also increase the burden of the decoder. In this work, a perceptual compression strategy based on interpretable kernel ensemble is proposed to improve the effective information density during the dimensionality compression stage.

Specifically, incorporating domain knowledge from fault diagnosis that the fault features in vibration signals usually appear as decay shocks [22], [23], [24], we design a convolution filter in the form of impact to extract the fault-related components of the vibration signal. Moreover, the features extracted are more physically interpretable and are understandable to humans. The interpretable layer performs the convolution operation with a predefined fault impact function that depends on two learnable parameters, and the form of the trainable impact kernels can be formulated by

$$S_{\text{conv}} = \cos(2\pi f_c \tau)\exp(-\delta\tau) + \lambda N \tag{15}$$

where f_c denotes the center frequency of the frequency band where the specified failure mode is located; δ is the decay parameter; τ represents the constant indicating the time scale of the kernel; $N$is the random normal variables; λ stands for the tradeoff parameters, and λ equals 0.1 in this work.

In the gradient back propagation process, the update process of the two parameters of the learnable impact kernel can be represented by

$$f_c^{i+1} = f_c^i - \eta\frac{\partial \mathcal{L}_{VQ}}{\partial f_c^i} \tag{16}$$

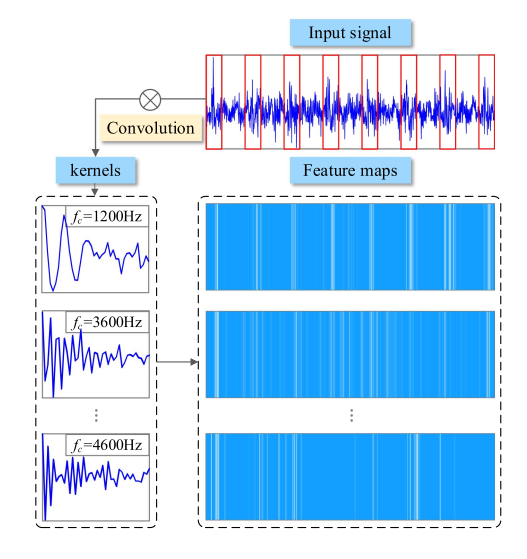


Fig. 3. Convolutional process of the input signals with interpretable convolution kernels. The red box indicates the fault impact position of the input signal. 1200 Hz is selected from the frequency band, in which the impact component is located. The white lines in the feature maps represent regions with higher energy.

$$\delta^{i+1} = \delta^i - \eta\frac{\partial \mathcal{L}_{VQ}}{\partial \delta^i} \tag{17}$$

where η denotes the learning rate; $\mathcal{L}_{VQ}$ represents the loss of the VQ-VAE; and ∂ is the derivative operator. We embed the interpretable impact kernels into the first layer of the VQ-VAE, then the perceptual compressed VQ-VAE is presented. The convolution process of the input signals with impact kernels can be visualized in Fig. 3.

C. The Optimization of IVQ-LDM

By consolidating the VQ-LDM and interpretable kernel, we provide an IVQ-LDM method for rotating machinery fault diagnosis with small data. The overall learning strategy can be summarized in Algorithm 1.

Algorithm 1: Training Procedure of IVQ-LDM.

Require input: Source data x; Diffusion step t; Class label y.
Require hyperparameters: Learning rate η; Maximum diffusion step T; Variance schedule β; Central frequency f_c; Decay parameter δ.

Stage I: Perceptual compression model pre-training.
For iteration = 1, 2, …, **do**
    Integrating the interpretable kernels and training VQ-VAE.
    Calculate $\mathcal{L}_{VQ}$ based on (13).
    Update the parameter of the VQ-VAE and interpretable kernels by backpropagation.
end for
Stage II: latent DDPM training
Get z_e through the encoder embedded the interpretable kernels.
Get z_q through vector quantization.
For iteration = 1, 2, …, **do**
    Get $z_{q,t}$ sampled from $q(z_{q,t}|z_{q,0})$, $t \sim Uniform(\{1, 2, \ldots, T\})$.
    Calculate $\mathcal{L}_{VQ-LDM}$ based on (14).
    Update denoising network parameters by $\theta \leftarrow \theta - \eta \nabla_\theta \mathcal{L}_{VQ-LDM}$.
end for
Stage III: Sampling
Get $z_{q,T}$ sampled from $p(z_{q,T})$.
For $t = T-1$, ……, 1, 0, **do**
    Get $z_{q,t-1}$ sampled from $p_\theta(z_{q,t-1}|z_{q,t}, y)$.
    $t \leftarrow t-1$.
end for
Return decoder ($z_{q,0} \leftarrow p_\theta(z_{q,0})$) back to the original dimension.

IV. Experiment Analysis

In this section, the performance of IVQ-LDM is evaluated on three datasets, meanwhile, several mainstream generative models are selected as competitors.

A. Experiment Data Description

1) Rolling Bearing (RB)-Bearing Dataset: To evaluate the performance of the IVQ-LDM, we experiment on the RB dataset from a test rig shown in Fig. 4. The experimental platform includes a driving motor, three support bearings, a torque transducer, a tested bearing, a radial hydraulic loading power unit, and an accelerometer. At the loading end, we applied a radial load of 1.5 KN to the tested bearing. During the testing, the speed of the motor is set to 1200 r/min. Using this platform, we collect data under six fault conditions with a sampling frequency of 10 kHz, which contains inner race crack (IRC), inner race wear (IRW), outer race crack (ORC), outer race wear (ORW), inner–outer race crack (IORC), and roller cage damage (RCD). For each faulty bearing, 40 samples are collected for data generation, each containing 2048 data points. After expanding the original bearing dataset, an additional 100 samples of each bearing are collected for testing the fault diagnosis model.

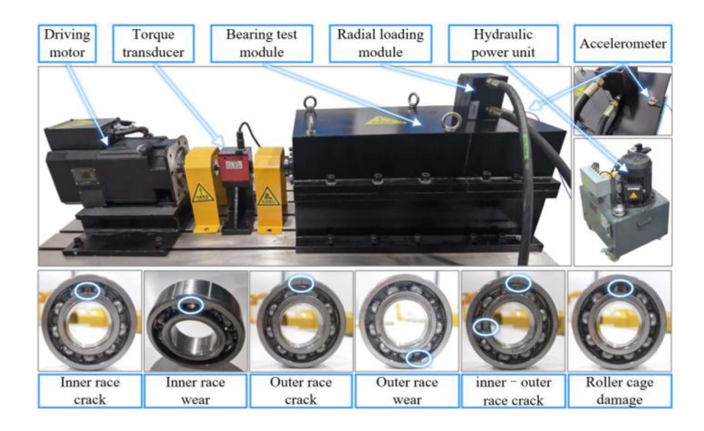


Fig. 4. RB-bearing test rig.

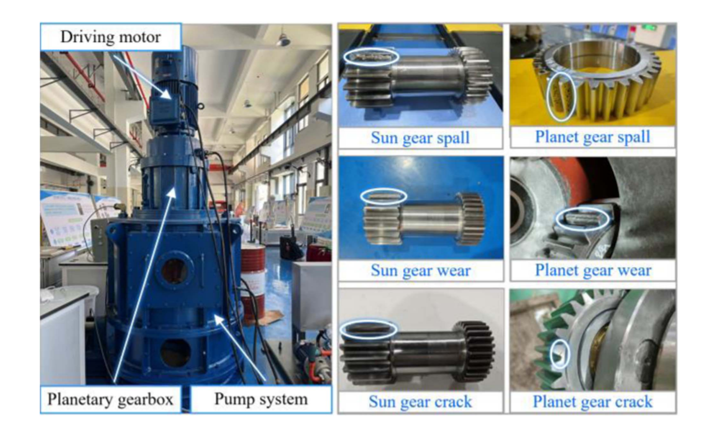


Fig. 5. Nuclear power planetary gearbox platform (scaling).

2) Planetary Gearbox (PG)-Gear Dataset: To further validate the effectiveness and applicability of the IVQ-LDM in real-world scenarios, we carried out the fault diagnosis experiments on a scaling nuclear power PG platform, as depicted in Fig. 5. The test rig is primarily composed of a driving motor, a tested PG, a pump system, and an accelerometer at a sampling frequency of 12.8 kHz attached to the gearbox. We test six typical failure modes, including sun gear spall (SGS), sun gear wear (SGW), sun gear crack (SGC), planet gear spall (PGS), planet gear wear (PGW), planet gear crack (PGC). The experiments are carried out under 746 r/min with a load proportion of 50%. In total, 40 samples of each failure mode are collected for training the generative models, with each sample having 4096 data points. At last, an additional 100 samples of each health state are collected for testing the fault diagnosis model.

3) KAt-Bearing Dataset: We choose an open-access bearing dataset from KAt-DataCenter of the Paderborn University [25] to evaluate the generality of the proposed method. As displayed in Fig. 6, the tested bearing is installed in the bearing module, and an accelerometer with a sampling frequency of 64 kHz is mounted on the bearing house. The data from six bearings with a speed of 1500 r/min, a torque of 0.7 N·m and a radial load of 1000 N are selected for our experiment. Specifically, the bearings

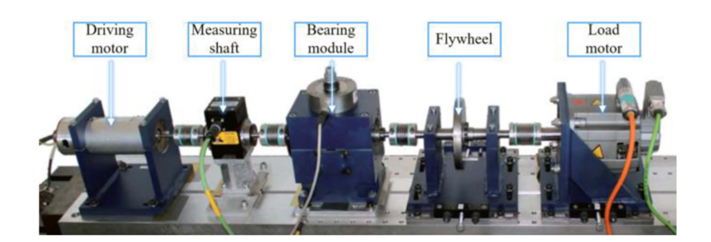


Fig. 6. KAt-bearing test rig.

TABLE I
TASK SETTING FOR DATA GENERATION AND FAULT DIAGNOSIS

Dataset	Training samples (Generation)	Testing samples (Diagnosis)	Sample length	Fault type
RB-bearing	40×6	100×6	2048	IRC, IRW, ORC, ORW, IORC, RCD
PG-gear	40×6	100×6	4096	SGS, SGW, SGC, PGS, PGW, PGC
KAt-bearing	40×6	100×6	4096	IR-1, IR-2, OR-1, OR-2, IOR-1, IOR-2

with real damage include incipient/severe inner ring pitting (IR-1/IR-2), outer ring pitting (OR-1/OR-2), and inner-outer ring pitting (IOR-1/IOR-2). 40 samples of each bearing are chosen for data generation, with each sample having 4096 data points. Finally, an additional 100 samples of each bearing are collected for evaluating the fault diagnosis model.

According to the three datasets, the data generation and fault diagnosis task settings are provided in Table I.

B. Compared Methods

To corroborate the superiority of the proposed method more convincingly, four mainstream methods are selected for comparison.

Generative adversarial network: GAN [10], a generative model based on the idea of adversarial games, generates new samples through the adversarial learning mechanism of the generator and discriminator.

Deep convolutional GAN (DCGAN): DCGAN [26] is a generative model with the convolutional neural network as its backbone. Both the generator and discriminator adopt the convolutional structures.

Auxiliary classifier GAN (ACGAN): ACGAN [27] improves the conditional generation performance of GAN by adding a classifier into the discriminator.

Wasserstein GAN with gradient penalty (WGAN-GP): WGAN-GP [28] is an improved version of the Wasserstein GAN, which is capable of producing more stable gradient descent paths and thus high-quality samples can be generated.

Vision transformer GAN (ViTGAN): ViTGAN [29] integrates the transformer architecture and employs regularization techniques to enhance its training stability.

DDPM: Denoising diffusion probabilistic model [16] is a generative model based on Markov processes. It captures the

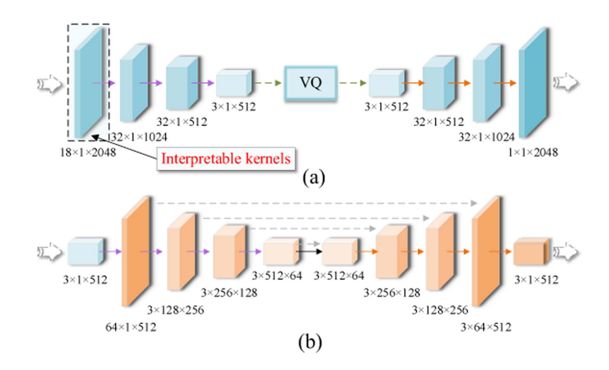


Fig. 7. Model structure of the IVQ-LDM. The length of input signal is 2048, which can be dynamically adjusted. (a) VQ-VAE. (b) Denoising U-net.

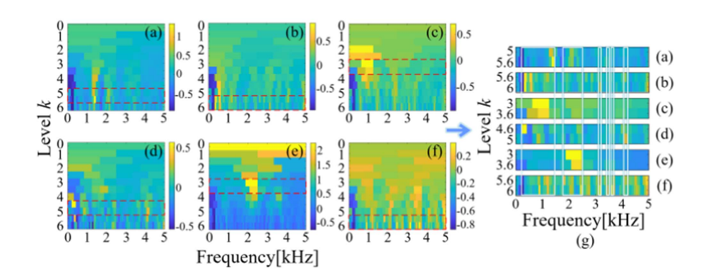


Fig. 8. Fast kurtogram of the bearings. (a) Kurtogram of IRC. (b) Kurtogram of IRW. (c) Kurtogram of ORC. (d) Kurtogram of ORW. (e) Kurtogram of IORC. (f) Kurtogram of RCD. (g) Selected band groups. The red dashed boxes indicate the filtered layers based on the kurtosis values, and the white boxes indicate the source bands of the selected central frequencies.

original data distribution by introducing the fine-grained destruction and reconstruction of the signal through the noise intervention, and thus can generate samples from random variables.

C. Implementation Details

The model structure of the IVQ-LDM is illustrated in Fig. 7. The latent DDPM is an eight-layer U-net structure, where the first four layers are downsampling convolution operations. The last four layers perform the upsampling convolution operations. Leaky rectified linear unit (LeakyReLU) is selected as the activation function. The length of each interpretable kernel is 40. As shown in Fig. 8, we select the central frequency through the fast kurtogram of the collected signal at each health state. Specifically, we integrate the frequency bands with higher kurtosis values and select the appropriate central frequency among them [as shown in Fig. 8(g)] to construct the interpretable kernels. Specifically, the selected central frequency of the RB-bearing dataset is {3, 3.5, 5, 5.5, 7, 9, 10, 13, 14, 19, 20, 21, 22, 23, 24, 31.5, 34.5, 36} $\times 10^2$. The central frequency of the PG-gear dataset is selected as {6, 22.5, 23, 25, 26, 27, 29, 33, 35, 36, 38, 39, 40, 41, 42, 45, 46, 47} $\times 10^2$. The central frequency of the KAt-bearing dataset is selected as {10, 11, 11.3, 13, 14, 15, 16, 16.6, 17.5, 18, 20, 21, 22, 23, 24, 25, 26.3, 28} $\times 10^3$.

We adopt the Adam optimization algorithm with learning rate $\eta = 1 \times 10^{-3}$ to train all the parameters of IVQ-LDM. The maximum training iteration times is set to 2000. The maximum

TABLE II
SELECTED HYPERPARAMETERS OF THE IVQ-LDM

Hyperparameter	Value
Learning rate η	Adam (0.001)
Max epochs	2000
Batch size	20
Max diffusion steps T	500
Variance schedule β	$(1\times10^{-4}, 0.02)$
Dimensionality compression ratio	4
Interpretable kernel length	40
Decay parameter δ	700

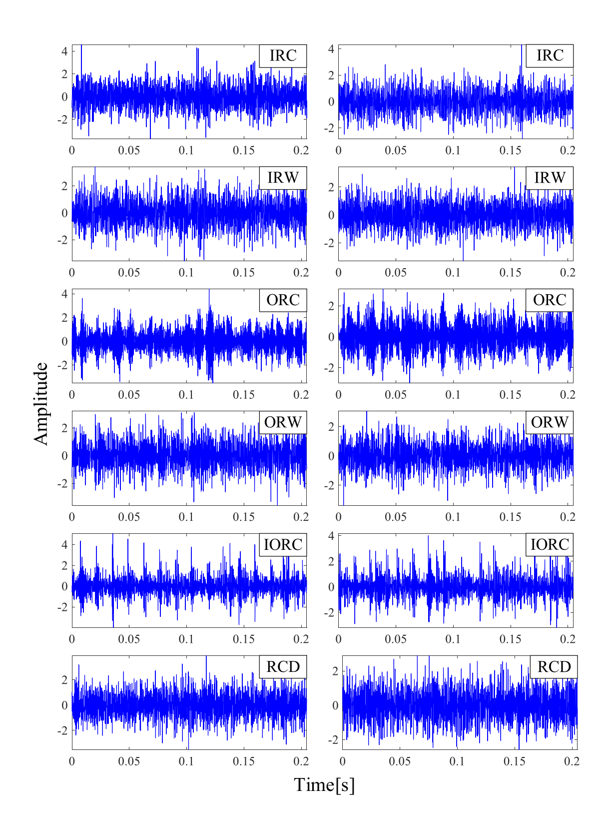


Fig. 9. RB-bearing data generation results based on the IVQ-LDM algorithm. Real data (left). Generated data (right).

diffusion steps T is set to 500. The variances increase linearly from $\beta_1 = 1 \times 10^{-4}$ to $\beta_T = 0.02$.

For an intuitive expression of the hyperparameter settings for IVQ-LDM, we have listed all the detailed parameter configurations in Table II. In addition, all experiments are conducted on Pytorch 1.9 framework with Python 3.8. All models are trained on an NVIDIA GeForce RTX Laptop 3070 GPU.

D. Quality Assessment of the Generated Signals

1) RB-Bearing Data Generation: The training samples from the RB-bearing dataset are utilized for training the IVQ-LDM to provide the synthesized vibration data for RB fault diagnosis. The comparison results of the real and generated signals for six fault states are depicted in Fig. 9. It can be seen that the vibration signals generated by IVQ-LDM are intuitively similar to the real signals. The frequency spectrum comparison between the real and generated signal is shown in Fig. 10. The spectrums of the synthesized signals exhibit favorable consistency with the real signals.

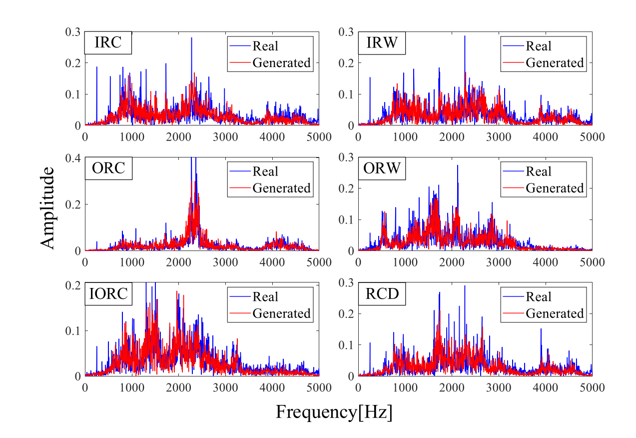


Fig. 10. Comparison of the frequency spectrum of the real and generated samples from the RB-bearing dataset.

TABLE III
EVALUATION RESULTS ON RB-BEARING DATA GENERATION

Methods	SCC↑	FD↓	RMSE↓	Training time (s)
Source-only	0.6804	0.8044	0.0251	-
GAN	0.3861	1.7473	0.0546	157
DCGAN	0.3561	1.1840	0.0370	285
ACGAN	0.3728	1.1808	0.0369	292
WGAN-GP	0.5391	1.0887	0.0322	162
ViTGAN	0.3202	1.0386	0.0324	1062
DDPM	0.5638	0.9767	0.0305	1462
IVQ-LDM	**0.6086**	**0.9663**	**0.0302**	**732**

The bold values indicate the results of the proposed method.

In addition to qualitative assessment, we leverage three similarity evaluation metrics to quantitatively analyze the quality of the generated signals, including Spearman correlation coefficient (SCC), Fréchet distance (FD), and root-mean-square error (RMSE). Considering the influence of the phase differences in time-domain signals, we assess the quality of data generation by calculating the similarity of the frequency spectrum. Specifically, we calculate the similarity among the original data as a reference, which we call Source-only. The comparison results for each method are detailed in Table III, where "↑" means larger is more similar and "↓" means smaller is more similar. The results of the proposed method are marked in bold. It can be observed that the diffusion generation techniques have improved the quality of data generation compared with the mainstream GAN-based approaches. In addition, with the dimensionality compression and interpretable kernel ensemble strategies, the IVQ-LDM achieved further enhancement in computing efficiency and data generation capacity. Compared with the DDPM, the IVQ-LDM obtains the best values across the three metrics, improving 7.9% (0.0448) and 1.1% (0.0104) on SCC and FD, respectively. More importantly, since learning in latent space, the IVQ-LDM reduces the training time by half compared to DDPM by about 12 min.

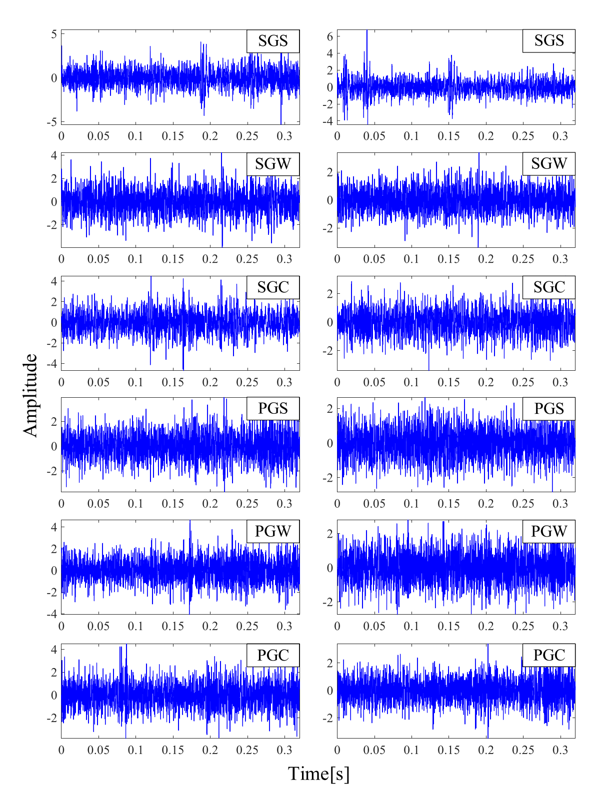


Fig. 11. PG-gear data generation results based on the IVQ-LDM algorithm. Real data (left). Generated data (right).

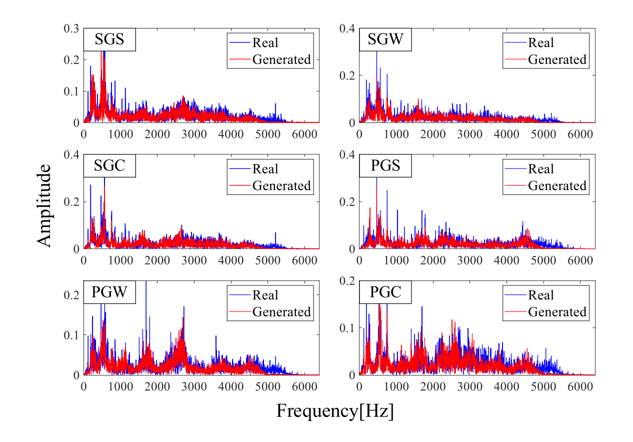


Fig. 12. Comparison of the frequency spectrum of the real and generated samples from the PG-gear dataset.

2) PG-Gear Data Generation: Data generation results of the proposed method on the PG-gear dataset are depicted in Figs. 11 and 12. These figures show that the synthesized data exhibit favorable diversity while maintaining the key structural features. Especially in the frequency spectrum, the consistency of the features between generated and raw signals could be more intuitively observed.

Similar to the quality evaluation process for RB-generated data, we also utilize SCC, FD, and RMSE to quantitatively assess the quality of the PG-generated data. The comparison results of the selected methods are presented in Table IV. Despite the higher computational cost of diffusion generation techniques compared with GAN-based generation methods, the data generation quality of diffusion generation approaches remains superior. The three metrics of the IVQ-LDM improve by more than 3.6% (0.0219), 3% (0.0292), and 2.9% (0.0006) compared with those of competitors. If pursuing the high-quality generated signal, diffusion generation techniques are undoubtedly the better choice. Furthermore, IVQ-LDM demonstrates superior performance compared with the classical DDPM, achieving improved data generation quality while reducing computational cost by approximately two times.

TABLE IV
EVALUATION RESULTS ON PG-GEAR DATA GENERATION

Methods	SCC↑	FD↓	RMSE↓	Training time (s)
Source-only	0.6494	0.9041	0.0200	-
GAN	0.3725	1.6692	0.0369	177
DCGAN	0.4304	1.0918	0.0241	312
ACGAN	0.4468	1.1045	0.0244	335
WGAN-GP	0.6018	1.0839	0.0239	174
ViTGAN	0.4436	1.0459	0.0231	1129
DDPM	0.5939	0.9690	0.0214	2289
IVQ-LDM	**0.6237**	**0.9398**	**0.0208**	**920**

The bold values indicate the results of the proposed method.

TABLE V
EVALUATION RESULTS ON KAT-BEARING DATA GENERATION

Methods	SCC↑	FD↓	RMSE↓	Training time (s)
Source-only	0.5517	0.8840	0.0195	-
GAN	0.3867	1.2861	0.0284	172
DCGAN	0.5036	1.2074	0.0267	335
ACGAN	0.4912	1.2074	0.0267	346
WGAN-GP	0.4797	1.1021	0.0243	189
ViTGAN	0.4075	1.2438	0.0275	1203
DDPM	0.5159	0.9258	0.0205	2276
IVQ-LDM	**0.5636**	**0.9210**	**0.0203**	**927**

The bold values indicate the results of the proposed method.

3) KAt-Bearing Data Generation: An additional experiment is carried out on a public KAt-bearing dataset to validate the generality of the proposed method. The evaluation results are detailed in Table V. We can see that diffusion-based methods are still significantly superior to the mainstream GAN-based methods. The improvement of IVQ-LDM in the three metrics is more than 11.9% (0.06), 16.4% (0.1811), and 16.4% (0.004) to mainstream GAN-based approaches, respectively. Besides, IVQ-LDM, which integrates the dimensionality compression technique, dramatically achieves a leading computational efficiency to the DDPM and ViTGAN by nearly 22 and 5 min, respectively. Therefore, the proposed methods could be better for some data generation tasks in fault diagnosis scenarios.

E. Fault Diagnosis Under Small Data

To verify the effectiveness of the IVQ-LDM in tackling the data-scarce problem, the RB-bearing, PG-gear, and KAt-bearing intelligent fault diagnosis experiments are carried out. We construct a 1-D convolutional neural network as the standard fault diagnosis model, which contains three convolutional layers and two fully-connected layers. Each convolution layer contains a

TABLE VI
TOTAL DIAGNOSIS RESULTS (%) ON THREE DATASETS

Methods	RB-bearing	PG-gear	KAt-bearing
Source-only	72.53 ± 1.96	79.81 ± 3.30	76.23 ± 2.70
GAN	60.53 ± 4.03	68.57± 3.54	71.87 ± 2.94
DCGAN	72.07 ± 3.23	77.21 ± 2.09	73.43 ± 2.38
ACGAN	73.00 ± 2.41	80.38 ± 2.06	75.93 ± 2.77
WGAN-GP	73.07 ± 2.07	74.43± 2.03	72.27 ± 1.77
ViTGAN	74.89 ± 2.03	77.80 ± 1.93	74.30 ± 2.98
DDPM	77.60 ± 2.00	85.33 ± 1.49	83.80 ± 1.73
IVQ-LDM	**84.78 ± 2.01**	**91.63 ± 1.31**	**91.50 ± 1.52**

The bold values indicate the results of the proposed method.

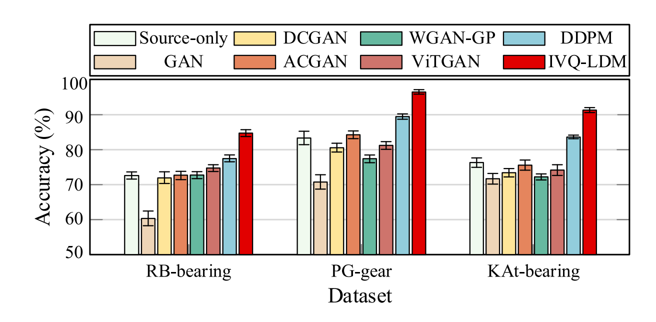


Fig. 13. Total fault diagnosis results on the three datasets.

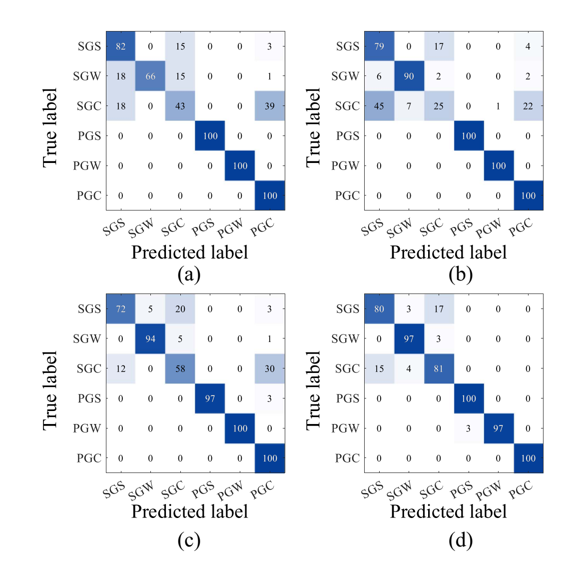


Fig. 14. Confusion matrix of the fault diagnosis results on PG-gear dataset. (a) Source-only. (b) ACGAN. (c) DDPM. (d) IVQ-LDM.

TABLE VII
FD ON ABLATION STUDY

Methods	RB-bearing	PG-gear	KAt-bearing
DDPM	0.9767	0.9690	0.9258
VQ-LDM	0.9736	0.9630	0.9257
IVQ-LDM	0.9663	0.9398	0.9210

TABLE VIII
DIAGNOSIS RESULTS (%) ON ABLATION STUDY

Methods	RB-bearing	PG-gear	KAt-bearing
DDPM	77.6	85.33	83.80
VQ-LDM	79.23 ↑1.63	86.34↑1.01	87.37 ↑3.57
IVQ-LDM	84.78 ↑7.18	91.63 ↑6.30	91.50 ↑7.70

convolution, a Maxpooling, a batch norm and a LeakyReLU activation operation. The size of the convolution kernel of the first and last two layers are 1×16 and 1×5, respectively.

The Adam optimization algorithm is adopted to train the intelligent fault diagnosis model, where the learning rate is set to 5×10^{-3}. We generate 40 samples for each health state and expand the original dataset from 40 samples per category to 80. Another 100 samples for each category are utilized for testing the diagnosis model. The fault diagnosis experiment for each method is repeated in five trials to eliminate the contingency.

The total diagnosis results for the three datasets are detailed in Table VI and Fig. 13. Although the original data volume has increased using GAN and DCGAN, the diagnosis accuracy is hindered due to the poor quality of the generated samples. Not only that, but other GAN-based methods also exhibit different degrees of impact on diagnosis performance across the three datasets. In contrast, the diffusion-based data generation techniques consistently have a significant improvement, especially the IVQ-LDM, which performs optimally regarding diagnosis accuracy and stability. The accuracy improvement to ACGAN and DDPM is about 11% and 6%, respectively, indicating the data generation quality of the proposed method. In addition, the confusion matrices of Source-only, ACGAN, DDPM, and IVQ-LDM on the PG-gear dataset are displayed in Fig. 14. Obvious misclassification cases can be found in source-only, ACGAN, and DDPM, further demonstrating the diagnosis superiority of the proposed method.

F. Analysis

1) Ablation Study: Compared with the conventional DDPM, two improved strategies are incorporated (i.e., VQ-VAE and Interpretable kernel) in IVQ-LDM. To further investigate the importance of each component, the ablation study on the DDPM, VQ-LDM, and IVQ-LDM is conducted. The results for data generation and fault diagnosis are respectively presented in Tables VII and VIII. From these results, we can see that each component plays a positive role. Specifically, the VQ-LDM improves the data generation quality while enhancing computational efficiency, indicating that latent space contains a higher density of valid information than the original. Furthermore, introducing interpretable kernels to retain more fault-related information in latent space shows a more significant performance upgrade, providing diagnosis accuracy gains of 7.18%, 6.3%, and 7.7%, respectively. In summary, the two-step strategy of enhancing the computational efficiency and the density of fault-related information does improve the performance of the DDPM.

2) Visualization of Interpretable Kernel: To provide a clear explanation of the interpretable layer, we carry out a visualization experiment to explore the difference between the conventional convolutional kernels and the interpretable impact kernels. The samples from IRC, ORC, SGS, and OR-2 are chosen as the model input, and the feature outputs of the first layer using the

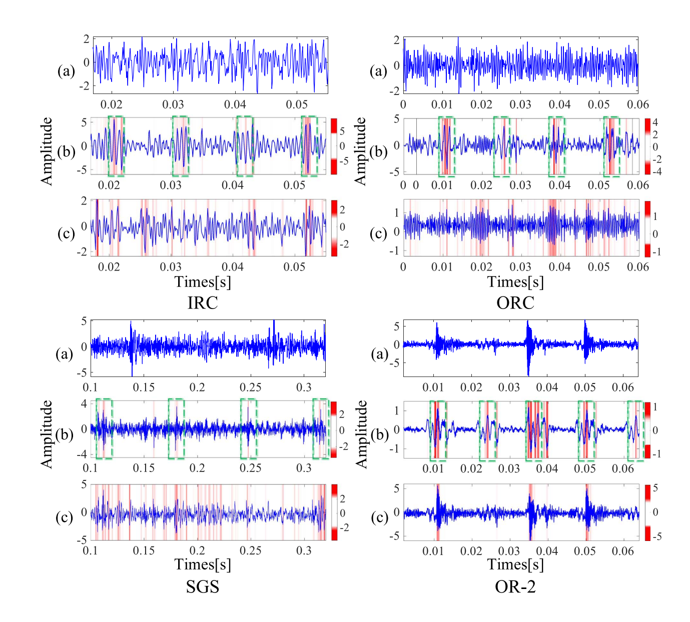


Fig. 15. Feature output of the interpretable kernel and convolutional kernel. Color bars indicate the correspondence between amplitude and color, the larger the amplitude the darker the color. The green dotted line indicates the impact location. (a) Original signal. (b) Output of the interpretable kernel. (c) Output of the convolutional kernel.

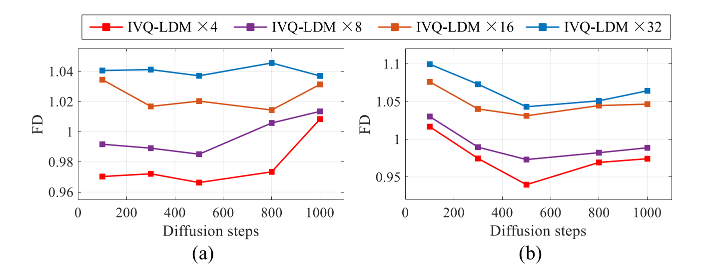


Fig. 16. Analyzing the quality of the generated signals with different compression factors r and diffusion steps T. (a) RB-bearing data generation experiment. (b) PG-gear data generation experiment.

two kinds of kernels are respectively obtained for comparison analysis. The total results are displayed in Fig. 15. Intuitively, the interpretable kernel allows for a better focus on the fault component (indicated by the green box) of the signal. On the contrary, due to the lack of fault diagnosis domain knowledge, the conventional convolutional kernel is challenging to uncover the potential fault information. In addition, the results show that the convolution kernel tends to extract features in an uninterpretable manner or even directly duplicate the input information, which can be evidently observed in Fig. 15 OR-2 (c). More importantly, the interpretable kernel not only extracts the fault impact with a high signal-to-noise ratio but also finds the weak fault component, which provides more fault-related information for the latent space. Therefore, the latent DDPM could be trained with a higher effective information density, further proving the effectiveness of the IVQ-LDM.

3) Compression Rate and Diffusion Steps Tradeoff: In order to explore the tradeoff between computational efficiency and the quality of generated signals, we analyze the performance of IVQ-LDM under different dimensionality compression factors $r \in \{4, 8, 16, 32\}$ and diffusion steps $T \in \{100, 300, 500, 800, 1000\}$, where IVQ-LDM$\times r$ corresponds to the compression rate of r times. Specifically, the larger compression factors and smaller diffusion steps lead to lower computational costs. The total experiment results are exhibited in Fig. 16. We can see that as the compression factors increase, the quality of generated data decreases linearly, especially in the RB-bearing experiment, where a significant performance drops at factors of $r \in \{16, 32\}$. Too strong compression rate resulting in information loss and thus limiting the achievable performance. In addition, under the same compression factor, the quality of the generated data would be affected by too few or too many diffusion steps. The IVQ-LDM exhibits favorable performance at most compression factors when the diffusion steps $T \in \{300, 500\}$. In summary, we can conclude that $r \in \{4, 8\}$ and $T \in \{300, 500\}$ lie in the best-behaved regime for pursuing high-quality synthesis results.

V. Conclusion

In this article, we introduce the concept of diffusion generation and present a novel method named IVQ-LDM for machinery fault diagnosis with data scarcity. Building upon the strengths of DDPM in data generation, we further designed and enhanced this approach in three aspects: data generation quality, computational efficiency, and interpretability. Specifically, we introduce the dimensionality compression technique of VQ-VAE to compress the original data into a lower dimensional space for enhancing computational efficiency. At the same time, the interpretable impact kernels are developed and integrated into the VQ-VAE to compress the original data perceptually, improving the density of fault-related information in the latent space. Finally, we construct a conditional DDPM in this space to learn the low-dimensional representation of the data. Furthermore, the proposed method is evaluated on three different mechanical systems compared to several mainstream data generation approaches. Our findings fully corroborate the superiority of the IVQ-LDM in data generation and fault diagnosis tasks. Specifically, The IVQ-LDM exhibits improvements of nearly or exceeding 0.02 in SCC and FD metrics to the competitors. The enhancement of diagnosis accuracy is more than 6%, reaching a maximum of 91.63%. Moreover, the computational efficiency is improved over one time to DDPM.

Additionally, two main research directions would be considered in future work. 1) although the introduction of IVQ-LDM has greatly improved the computational efficiency, its computational cost is still higher than the conventional methods. Given this, we plan to improve the network architecture of DDPM by introducing the knowledge distillation and model pruning strategy in future work. 2) The interpretable impact kernel brings positive gains for fault data generation in this work. However, studying the deeper layer interpretable for generative models is still challenging. In future work, we will investigate how embedding the fault diagnosis domain knowledge into deep layers while exploring the driving factors for improving the quality of data generation. We also expect the diffusion generation technique would serve more in the field of industrial equipment fault diagnosis.

References

[1] Z. Gao, C. Cecati, and S. X. Ding, "A survey of fault diagnosis and fault-tolerant techniques—Part I: Fault diagnosis with model-based and signal-based approaches," *IEEE Trans. Ind. Electron.*, vol. 62, no. 6, pp. 3757–3767, Jun. 2015.

[2] Y. Lei, B. Yang, X. Jiang, F. Jia, N. Li, and A. K. Nandi, "Applications of machine learning to machine fault diagnosis: A review and roadmap," *Mech. Syst. Signal Process.*, vol. 138, 2020, Art. no. 106587.

[3] J. Jiao, H. Li, T. Zhang, and J. Lin, "Source-Free adaptation diagnosis for rotating machinery," *IEEE Trans. Ind. Inform.*, vol. 19, no. 9, pp. 9586–9595, Sep. 2023.

[4] J. Jiao, M. Zhao, J. Lin, and K. Liang, "A comprehensive review on convolutional neural network in machine fault diagnosis," *Neurocomputing*, vol. 417, pp. 36–63, 2020.

[5] H. Shao, M. Xia, G. Han, Y. Zhang, and J. Wan, "Intelligent fault diagnosis of rotor-bearing system under varying working conditions with modified transfer convolutional neural network and thermal images," *IEEE Trans. Ind. Informat.*, vol. 17, no. 5, pp. 3488–3496, May 2021.

[6] Y. Hu, R. Liu, X. Li, D. Chen, and Q. Hu, "Task-Sequencing meta learning for intelligent Few-Shot fault diagnosis with limited data," *IEEE Trans. Ind. Informat.*, vol. 18, no. 6, pp. 3894–3904, Jun. 2022.

[7] S. R. Saufi, Z. A. bin Ahmad, M. S. Leong, and M. H. Lim, "Gearbox Fault Diagnosis Using a Deep Learning Model with Limited Data Sample," *IEEE Trans. Ind. Informat.*, vol. 16, no. 10, pp. 6263–6271, Oct. 2020.

[8] T. Zhang, J. Jiao, J. Lin, H. Li, J. Hua, and D. He, "Uncertainty-based contrastive prototype-matching network towards cross-domain fault diagnosis with small data," *Knowl.-Based Syst*, vol. 254, Oct. 2022, Art. no. 109651.

[9] B. Dai and W. David, "Diagnosing and Enhancing VAE models," 2019, *arXiv:1903.05789*. [Online]. Available: https://arxiv.org/abs/1903.05789

[10] I. Goodfellow et al., "Generative adversarial networks," *Adv. Neural Inf. Process. Syst.*, vol. 2, pp. 2672–2680, 2014.

[11] T. Pan, J. Chen, T. Zhang, S. Liu, S. He, and H. Lv, "Generative adversarial network in mechanical fault diagnosis under small sample: A systematic review on applications and future perspectives," *ISA Trans.*, vol. 128, Part. B, pp. 1–10, Sep. 2022.

[12] S. Liu, H. Jiang, Z. Wu, and X. Li, "Data synthesis using deep feature enhanced generative adversarial networks for rolling bearing imbalanced fault diagnosis," *Mech. Syst. Signal Process.*, vol. 163, 2022, Art. no. 108139.

[13] H. Shao, W. Li, B. Cai, J. Wan, and S. Member, "Dual-threshold attention-guided GAN and limited infrared thermal images for rotating machinery fault diagnosis under speed fluctuation," *IEEE Trans. Ind. Inform.*, vol. 19, no. 9, pp. 9933–9942, Sep. 2023.

[14] K. Zhang, Q. Chen, J. Chen, S. He, F. Li, and Z. Zhou, "A multi-module generative adversarial network augmented with adaptive decoupling strategy for intelligent fault diagnosis of machines with small sample," *Knowl.-Based Syst.*, vol. 239, 2022, Art. no. 107980.

[15] T. Salimans, I. Goodfellow, W. Zaremba, V. Cheung, A. Radford, and X. Chen, "Improved Techniques for Training GANs," *Adv. Neural Inf. Process. Syst.*, vol. 29, pp. 2234–2242, 2016.

[16] J. Ho, A. Jain, and P. Abbeel, "Denoising Diffusion Probabilistic Models," *Adv. Neural Inf. Process. Syst.*, vol. 33, pp. 6840–6851, Jun. 2020.

[17] P. Dhariwal and A. Nichol, "Diffusion Models Beat GANs on Image Synthesis," *Adv. Neural Inf. Process. Syst.*, vol. 34, pp. 8780–8794, 2021.

[18] R. Rombach, A. Blattmann, D. Lorenz, and P. Esser, "High-Resolution Image Synthesis with Latent Diffusion Models," in *Proc. IEEE Conf. Comput. Vis. Pattern Recognit.*, 2022, pp. 10684–10695.

[19] O. Vinyals and K. Kavukcuoglu, "Neural Discrete Representation Learning," *Adv. Neural Inf. Process. Syst.*, vol. 30, pp. 6309–6318, 2017.

[20] M. Ravanelli and Y. Bengio, "Interpretable Convolutional Filters with SincNet," Nov. 2018, *arXiv:1811.09725*. [Online]. Available: https://arxiv.org/abs/1811.09725

[21] H. Zhang, J. Lin, J. Hua, and T. Tong, "Interpretable convolutional sparse coding method of Lamb waves for damage identification and localization," *Struct. Health Monit.*, vol. 21, no. 4, pp. 1790–1804, 2022.

[22] K. Zhang, P. Chen, M. Yang, L. Song, and Y. Xu, "The Harmogram: A periodic impulses detection method and its application in bearing fault diagnosis," *Mech. Syst. Signal Process.*, vol. 165, Feb. 2022, Art. no. 108374.

[23] X. Zhang et al., "Feature enhancement based on regular sparse model for planetary gearbox fault diagnosis," *IEEE Trans. Instrum. Meas.*, vol. 71, May 2022, Art. no. 3514316.

[24] M. Zhao and X. Jia, "A novel strategy for signal denoising using reweighted SVD and its applications to weak fault feature enhancement of rotating machinery," *Mech. Syst. Signal Process.*, vol. 94, pp. 129–147, 2017.

[25] C. Lessmeier, J. K. Kimotho, D. Zimmer, and W. Sextro, "Condition monitoring of bearing damage in electromechanical drive systems by using motor current signals of electric motors: A benchmark data set for data-driven classification," in *Proc. Eur. Conf. Prognostics Health Manage. Soc.*, 2016, pp. 1–17.

[26] A. Radford, L. Metz, and S. Chintala, "Unsupervised Representation Learning with Deep Convolutional Generative Adversarial Networks," Nov. 2015, *arXiv: 1511.06434*. [Online]. Available: https://arxiv.org/abs/1511.06434

[27] A. Odena, O. Christopher, and S. Jonathon, "Conditional image synthesis with auxiliary classifier gans," in *Proc. 34th Int. Conf. Machin. Learn. PMLR.*, 2017, pp. 2642–2651.

[28] I. Gulrajani, F. Ahmed, M. Arjovsky, V. Dumoulin, and A. Courville, "Improved Training of Wasserstein GANs," *Adv. Neural Inf. Process. Syst.*, vol. 30, pp. 5768–5778, Mar. 2017.

[29] K. Lee, H. Chang, L. Jiang, H. Zhang, Z. Tu, and C. Liu, "Vitgan: Training gans with vision transformers," 2021, *arXiv: 2107.04589*. [Online]. Available: https://arxiv.org/abs/2107.04589



Tian Zhang received the B.S. degree in mechanical design, manufacture, and automation from Nanchang Hangkong University, Nanchang, China, in 2019. He is currently working toward the Ph.D. degree in electronic information with the School of Reliability and Systems Engineering, Beihang University, Beijing, China.

His current research interests include few-shot learning, interpretable deep learning, and intelligent fault diagnosis and prognosis of complex mechanical systems.



Jing Lin (Senior Member, IEEE) received the B.S., M.S. and Ph.D. degrees in mechanical engineering from Xi'an Jiaotong University, Xi'an, China, in 1993, 1996, and 1999, respectively.

From 2009 to 2018, he was a Professor with the School of Mechanical Engineering, Xi'an Jiaotong University. He is currently the Dean with the School of Reliability and Systems Engineering, Beihang University, Beijing, China. He is also the Changjiang Distinguished Professor with the Ministry of Education of China, Beijing, China. His current research field includes machinery condition monitoring, fault diagnosis and prognosis, vibration analysis, and nonstationary signal processing.

Dr. Lin was the recipient of the Distinguished Young Scholar Funding from the National Natural Science Fund in 2011 and won the State Natural Science Award in 2013.



Jinyang Jiao (Member, IEEE) received the B.S. degree in vehicle engineering from the China University of Petroleum, Qingdao, China, in 2015, and the Ph.D. degree in mechanical engineering from Xi'an Jiaotong University, Xi'an, China, in 2020.

From 2019 to 2020, he was a Visiting Ph.D. Student with the Department of Mechanical and Industrial Engineering, University of Toronto, Toronto, ON, Canada. He is currently an Associate Professor with the School of Reliability and Systems Engineering, Beihang University, Beijing, China. His research interests include transfer learning, data analytics, machinery condition monitoring, and intelligent fault diagnosis.



Han Zhang received the B.S. degree in measurement and control technology and instrument from Beijing Jiaotong University, Beijing, China, in 2018, and the Ph.D. degree in systems engineering from Beihang University, Beijing, China, in 2023.

She is currently a Postdoctor with the Institute of Mechanics and Acoustics, National Institute of Metrology, Beijing. Her research interests include deep learning, nondestructive testing, and vibration metrology.



Hao Li received the B.S. degree in safety engineering in 2020 from Beihang University, Beijing, China, where he is currently working toward the Ph.D. degree in systems engineering with the School of Reliability and Systems Engineering.

His current research interests include signal processing and deep learning for mechanical fault diagnosis and prognosis.